Structural and biochemical basis for selective repression of the orphan nuclear receptor liver receptor homolog 1 by small heterodimer partner

Yong Li*, Mihwa Choi†, Kelly Suino*, Amanda Kovach*, Jennifer Daugherty*, Steven A. Kliewer†, and H. Eric Xu*‡

*Laboratory of Structural Sciences, Van Andel Research Institute, 333 Bostwick Avenue, Grand Rapids, MI 49503; and †Departments of Molecular Biology and Pharmacology, University of Texas Southwestern Medical School, 5323 Harry Hines Boulevard, Dallas, TX 75235

Edited by Jan-Åke Gustafsson, Karolinska Institute, Huddinge, Sweden, and approved May 15, 2005 (received for review February 11, 2005)

The functional interaction between the orphan nuclear receptors small heterodimer partner (SHP) and liver receptor homolog 1 (LRH-1), where SHP binds to LRH-1 and represses its constitutive transcriptional activity, is crucial for regulating genes involved in cholesterol homeostasis. Here, we report structural and biochemical analyses of the LRH-1/SHP interaction. The crystal structure and modeling studies of the LRH-1 ligand-binding domain bound to either of the two LXXLL-related motifs of SHP show that the receptor undergoes conformational changes to accommodate the SHP docking and reveal key residues that determine the potency and selectivity of SHP binding. Through a combination of mutagenesis and binding studies, we demonstrate that only the second SHP LXXLL motif is required for repressing LRH-1, and this motif displays a strong preference for binding to LRH-1 over the closely related receptor steroidogeneic factor 1 (SF-1). Structural comparisons indicate that this binding selectivity is determined by residues flanking the core LXXLL motifs. These results establish a structural model for understanding how SHP interacts with LRH-1 to regulate cholesterol homeostasis and provide new insights into how nuclear receptor/coregulator selectivity is achieved.

steroidogeneic factor 1 | bile acids | coactivators | corepressors

Liver receptor homolog 1 (LRH-1, NR5A2) is an orphan nuclear receptor that activates an array of genes responsible for development of endodermal organs such as liver, intestine, and pancreas (reviewed in ref. 1). LRH-1 also plays a central role in lipid homeostasis by regulating genes involved in bile acid synthesis, reverse cholesterol transport, and metabolism of lipoprotein complexes (2–6). In the nuclear receptor superfamily, LRH-1 is most homologous to steroidogeneic factor 1 (SF-1, NR5A1), which is essential for sex differentiation and development of adrenals and gonads (7, 8). LRH-1 and SF-1 share a highly conserved DNA-binding domain (DBD, >90% identity) and a moderately conserved ligand-binding domain (LBD, 56% identity). In contrast to most other nuclear receptors that function as dimers, LRH-1 and SF-1 bind with high affinity as monomers to a conserved consensus DNA site found in the promoters of target genes (9). The high degree of similarity in the DBDs of LRH-1 and SF-1 suggests that their different biological activities are contributed in part by distinct structural features in their LBDs, which recruit specific cofactors to regulate transcription.

LRH-1 seems to be a constitutively active transcription factor in that it activates many reporters in the absence of any exogenous ligands. The crystal structure of the mouse LRH-1 LBD reveals a sandwich fold of four layers of helices instead of the three layers observed for many other receptors (10). Despite the absence of any ligand in the large ligand-binding pocket, the C-terminal activation helix (AF-2) of LRH-1 is packed in an active conformation. The constitutive LRH-1 activity is proposed to be the result of the stabilization of the canonical LBD by the extended helix 2, which comprises the fourth layer of the helix sandwich fold. *In vivo*, the constitutive activity of LRH-1 is regulated by another orphan receptor SHP (small heterodimer partner, NR0B2), which contains a putative LBD but lacks a traditional DNA-binding domain (2, 3, 11). SHP was originally identified as a corepressor that interacts with a number of nuclear receptors, including peroxisome proliferator-activated receptors (PPARs), estrogen receptors, retinoid-X receptors, and LRH-1 (12–15). The physiological significance of the LRH-1/SHP interaction is well illustrated by its role in the negative feedback regulation of the cholesterol 7-α-hydroxylase gene (CYP7A1), which encodes the rate-limiting enzyme in the conversion of hepatic cholesterol to bile acids (2, 3). Activation of the bile acid receptor, FXR, causes an increase in SHP, which in turn interacts with LRH-1 bound to the CYP7A1 promoter and blocks its stimulatory effects on transcription (2, 3, 16). The SHP gene itself is also regulated by LRH-1 (2, 3, 16). Thus, bile acid homeostasis is regulated at multiple levels by a complex regulatory cascade involving FXR, LRH-1, and SHP, in which SHP/LRH-1 interactions play a pivotal role.

SHP employs two functional AF-2-binding motifs, which closely resemble the LXXLL motifs found in a large number of nuclear receptor AF-2 coregulators including the PPARγ coactivator (PGC-1α) and the steroid receptor coactivators (the SRC/p160 coactivator family), to interact with the LBDs of nuclear receptors (17). Although the physical regions of SHP that interact with LRH-1 have not been mapped, it is assumed that SHP uses the same LXXLL-related motifs to interact with LRH-1. However, previous structural and mutagenesis studies indicate that the LRH-1 structure is not suitable for optimal binding of an LXXLL coactivator motif (10, 18). Thus, the molecular basis for the LRH-1/SHP interaction remains unclear. In addition, the reason why SHP inhibits LRH-1 but not SF-1 is not fully understood (3). In this report, we have performed structural and biochemical analyses to probe the LRH-1/SHP interaction. Our results provide critical insights into why SHP preferentially represses LRH-1.

Methods

Protein Preparation and Crystallization. The mouse LRH-1 LBD (residues 318–560) was expressed in *Escherichia coli* and was complexed with SHP ID1 and ID2 peptides for crystallization with details described in *Supporting Methods*, which is published as supporting information on the PNAS web site.

Data Collection, Structure Determination, and Refinement. Data were collected at the ID line of sector-32 of the Advanced

This paper was submitted directly (Track II) to the PNAS office.

Freely available online through the PNAS open access option.

Abbreviations: LRH-1, liver receptor homolog 1; SF-1, steroidogeneic factor 1; LBD, ligand-binding domain; SHP, small heterodimer partner; PPAR, peroxisome proliferator-activated receptor; SRC, steroid receptor coactivator.

Data deposition: The atomic coordinates and structure factors have been deposited in the Protein Data Bank, www.pdb.org [PDB ID codes 1ZH7 (LRH-1/SHP ID1 binary complex) and 1ZGY (PPARγ/rosiglitazone/SHP ID2 ternary complex)].

‡To whom correspondence should be addressed. E-mail: eric.xu@vai.org.

Photon Source, and were processed with HKL2000 (19). The structures were determined by molecular replacement by using apo LRH-1 (10) or PPARγ/rosiglitazone (20) as a model with the AMORE program (21), and refined with CNS (22).

Binding Assays. The binding of the cofactor motifs to the nuclear receptors was determined by AlphaScreen assays as described (23, 24). The peptide sequences and the AlphaScreen procedures are detailed in *Supporting Methods*.

Transient Transfection Assays. The expression plasmids for the mouse receptors (LRH-1, SF-1, SHP, and Dax-1) and an SF-1/LRH-1 reporter plasmid were used in transfection assays with details described in *Supporting Methods*.

Results

Selective Binding of the SHP LXXLL-Related Motifs to LRH-1. The two SHP LXXLL-related motifs (ID1 and ID2 in Fig. 1*A*) are crucial for repression of a number of nuclear receptors in reporter assays (17). To test the direct binding of the SHP LXXLL motifs to LRH-1, we used biotinylated SHP ID1 and ID2 peptides to measure their interactions with the purified LRH-1 LBD using AlphaScreen assays (23, 24). In this assay, donor and acceptor beads were attached to the SHP peptides and the LRH-1 protein, respectively. When the SHP peptides interact with LRH-1, excitation with a laser beam at 680 nm causes the donor bead to emit single oxygen molecules that activate the fluorophores in the acceptor bead, and light is recorded at 520–620 nm. As shown in Fig. 1*B*, incubation of LRH-1 and the SHP ID1 peptide yielded ≈30,000 photon counts versus <200 photon counts produced by either LRH-1 or the SHP ID1 peptide alone, demonstrating the binding of the SHP ID1 peptide to the receptor. Purified LRH-1 was also able to interact with the SHP ID2 motif as well as the LXXLL motifs from coactivators PGC1α, CBP, TRAP220, SRC-1, and TIF2 but not with the corepressor motifs from SMRT and N-CoR.

To determine the affinities of SHP ID1 and ID2 binding to LRH-1, we performed peptide competition experiments using unlabeled SHP ID1 and ID2 peptides. Both the SHP ID1 and ID2 bind to LRH-1 with an IC_{50} of ≈0.5 μM (Fig. 1*C*). We also measured the binding affinity of the second LXXLL motifs of SRC-1 and TIF2, which bind to LRH-1 with IC_{50} values of 50 nM and 8.0 μM, respectively. These quantitative measurements reveal that the affinities for SHP ID1 and ID2 binding to LRH-1 are comparable with those of coactivator motifs.

Because SHP has been reported to repress the activation of a number of nuclear receptors (14, 25–27), we determined the relative binding affinity of the two SHP motifs to several receptors by using 500 nM SHP ID1 or ID2 peptide in the peptide competition experiments. As shown in Fig. 1*D*, the presence of 500 nM either SHP ID1 or ID2 peptide inhibited binding of the TIF2 LXXLL motif to LRH-1 by 50%, which is consistent with the binding affinity (IC_{50}) of these two SHP motifs to LRH-1 as shown in Fig. 1*C*. The presence of the same amount of the SHP peptides inhibited binding of the TIF2 coactivator motif to other purified receptors [including SF-1, PPARs, hepatocyte nuclear factor 4α (HNF4α), ERα, ERβ, and oxosteroid hormone receptors] by only 5–25% [except for RXR, which is inhibited ≈50% by SHP ID1]. These results demonstrate that the SHP LXXLL motifs, especially the second motif (ID2), preferentially interact with LRH-1 among all receptors tested.

Crystal Structure of the LRH-1/SHP ID1 Complex. To determine the molecular basis for the LRH/SHP interaction, we attempted to crystallize the LRH-1 LBD in a complex with the SHP ID1 or ID2 peptide. The LRH-1/SHP ID2 complex failed to crystallize, but LRH-1/SHP ID1 crystals were readily obtained in the C_2 space group with two complexes in each asymmetry unit. The statistics for the datasets and the refined 2.5-Å structures are summarized in Table 1, which is published as supporting information on the PNAS web site. Fig. 2 *A* and *B* shows two 90-degree views of the overall arrangement of the LRH-1/SHP ID1 complex. The LRH-1 LBD adopts a four-layered helical sandwich fold that closely resembles the LRH-1 apo LBD structure. As seen with the apo LBD structure,

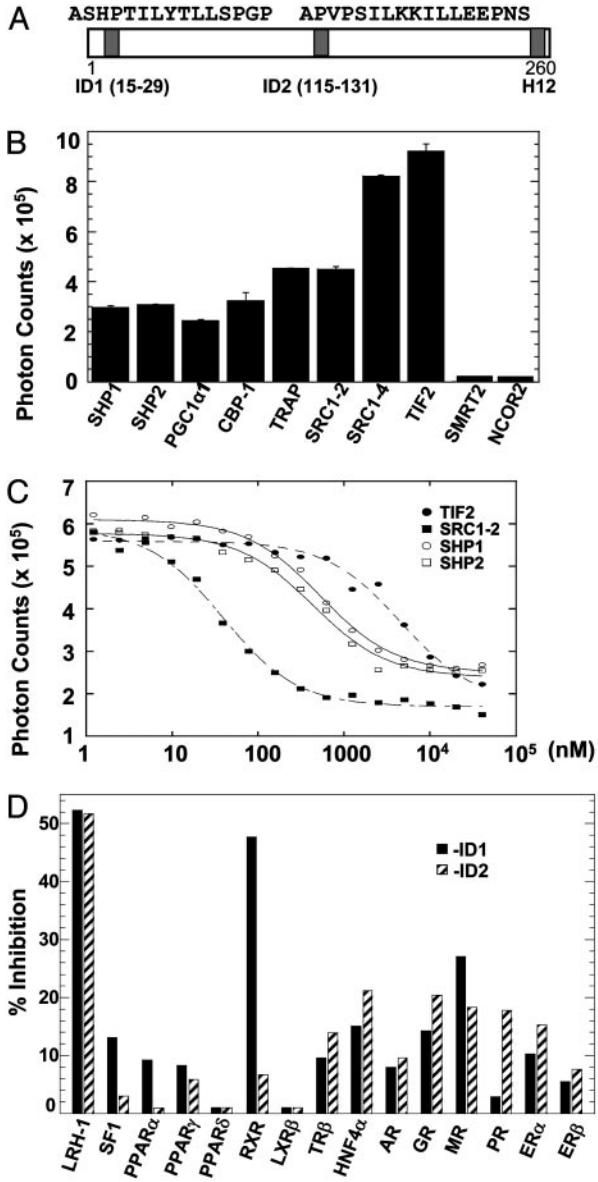

Fig. 1. Binding of the SHP LXXLL-related motifs to LRH-1. (*A*) A schematic representation showing the SHP protein and its two receptor-interacting motifs (ID1 and ID2), which were used in cocrystallization with LRH-1 and PPARγ. The sequences were adopted from Johansson *et al.* (17). (*B*) Binding of various LXXLL motifs to the purified LRH-1-1 LBD as measured by AlphaScreen assays. The background reading of either LRH-1 or the peptides alone is <200. (*C*) Binding affinity of LRH-1 with the SHP ID1 and ID2 motifs and coactivator LXXLL motifs is determined by IC_{50} values from peptide competitions of the binding of the TIF2 third motif to LRH-1 as measured by AlphaScreen assays. (*D*) The relative binding affinity of the SHP motifs to various purified receptor LBDs is measured by AlphaScreen assays by using 500 nM SHP ID1 and ID2 peptides to compete off the binding of the TIF2 third motif to the receptors. A 0% inhibition is the reading in the absence of any competing peptide where 100% inhibition represents the reading in the presence of 100 μM TIF2 peptide. GR, glucocorticoid receptor; MR, mineralocorticoid receptor; AR, androgen receptor, ER, estrogen receptor; PR, progesterone receptor; TR, thyroid hormone receptor.

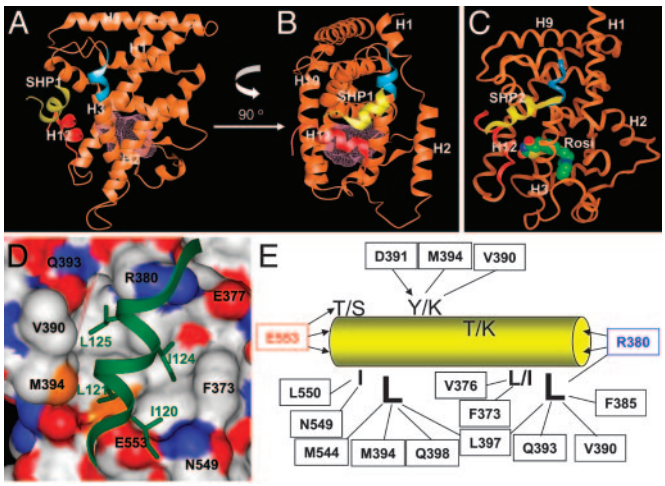

Fig. 2. Structure of LRH-1 bound to the SHP LXXLL motifs. (*A* and *B*) Two 90-degree views of the LRH-1/SHP ID1 complex in ribbon representation. LRH-1 is colored in gold with its charged clamp residues colored in red (AF-2) and blue (end of H3). The SHP ID1 peptide is in yellow, and the LRH-1 ligand-binding pocket is represented by a pink surface. (*C*) The overall structure of the PPARγ/rosiglitazone/SHP ID2 ternary complex. PPARγ is colored in gold with its charged clamp residues colored in red (AF-2) and blue (end of H3). The SHP is in yellow, and rosiglitazone is shown in space filling. (*D*) Docking of the SHP ID2 motif (green) on the LRH-1 coactivator-binding site is shown in surface representation. (*E*) A schematic representation depicting the intermolecular interactions of the SHP ID1 and ID2 motifs with LRH-1.

the SHP-bound LRH-1 also contains a large binding pocket with a cavity volume of ≈800 Å^3, but the pocket is empty. Despite the empty pocket, the C-terminal AF-2 is positioned in the active conformation as in the apo structure. The rms deviation (rmsd) of Cα atoms between the apo- and the SHP-bound LRH-1 structures is 0.45 Å (Fig. 3*A*). The major difference is the stability of the extended helix H2, which is partially disordered toward its C terminus in both LRH-1/SHP complexes in our crystals.

The docking mode of the SHP ID1 is well defined in the LRH-1/SHP interface. The ILYTLL sequence of the SHP ID1 adopts a two-turn amphipathic α-helix with L21 and L25 oriented inward toward the LRH-1 surface, and I20 and L24 partially exposed to solvent (Fig. 3*E*). Like other nuclear receptor-coactivator interactions, LRH-1 uses two "charge clamp" residues (E553 from the AF2 and R380 from helix 3) to mediate a series of hydrogen bonds with the backbone dipole of the SHP ID1 helix. The charge clamp residue from helix 3, which is normally a lysine in other receptors, is an arginine in LRH-1. The larger side chain of R380 pushes the SHP helix outward by 1.0–1.6 Å. The docking of the SHP ID1 helix is further stabilized by interactions of several other residues with LRH-1, which are summarized in Fig. 2*E*.

Structural Model of the LRH-1/SHP ID2 Complex. We were unable to crystallize the LRH-1/SHP ID2 complex despite numerous attempts. Because the SHP ID2 motif interacts with other nuclear receptors, although with lower affinity (Fig. 1*D*), we crystallized SHP ID2 bound to the PPARγ LBD in the presence of the agonist rosiglitazone. The structure of the PPARγ/SHP ID2 complex was determined and refined at 1.8 Å, a resolution that permits the unambiguous determination of the docking mode of the SHP ID2 motif (Fig. 2*C*). Like the coactivator LXXLL motif, the core ILKKIL motif of the SHP ID2 peptide adopts a two-turn α-helix with L121 and L125 directed toward the center interface of receptor, and residues I120 and I124 oriented at a 90-degree angle to the center interface. Overall, the interactions of the SHP ID2 peptide with PPARγ are analogous to those observed in the SRC-1-bound PPARγ structure (20, 28), and there is not a significant conformational difference between these two structures.

The availability of both the LRH-1/SHP ID1 and the PPARγ/SHP ID2 complexes provides an accurate template for modeling the interactions between the SHP ID2 motif and LRH-1. Superposition of the PPARγ/SHP ID2 complex with the LRH-1/SHP ID1 complex indicates that the SHP ID2 helix would fit snuggly into the SHP ID1-binding site of the LRH-1 without any additional movement of the LRH-1 residues (Fig. 2*D*). In this model, the interactions of the SHP ID2 with LRH-1 resemble those mediated by the SHP ID1. Residues L121 and L125 of the SHP ID2 motif mimic L21 and L25 of the SHP ID1 motif and mediate the core interactions with LRH-1 (Fig. 2*E*). Residue K122 is extended to form a unique hydrogen bond with LRH-1 D391, which is analogous to the R + 2 charge clamp interaction of the third TIF2 LXXLL motif in the GR and CAR cocrystal structures (24, 29).

LRH-1 Conformational Changes Induced by SHP Binding. Although there is no major rearrangement in the overall backbone structure or the ligand-binding pocket of LRH-1 (Fig. 3*A*), the binding of the SHP ID1 peptide induces a series of conformational changes in the LRH-1 side chains that contact SHP. These conformational changes are apparent when the LRH/SHP complex is overlaid on the apo structure (Fig. 3 *B–D*). The most dramatic change is the side

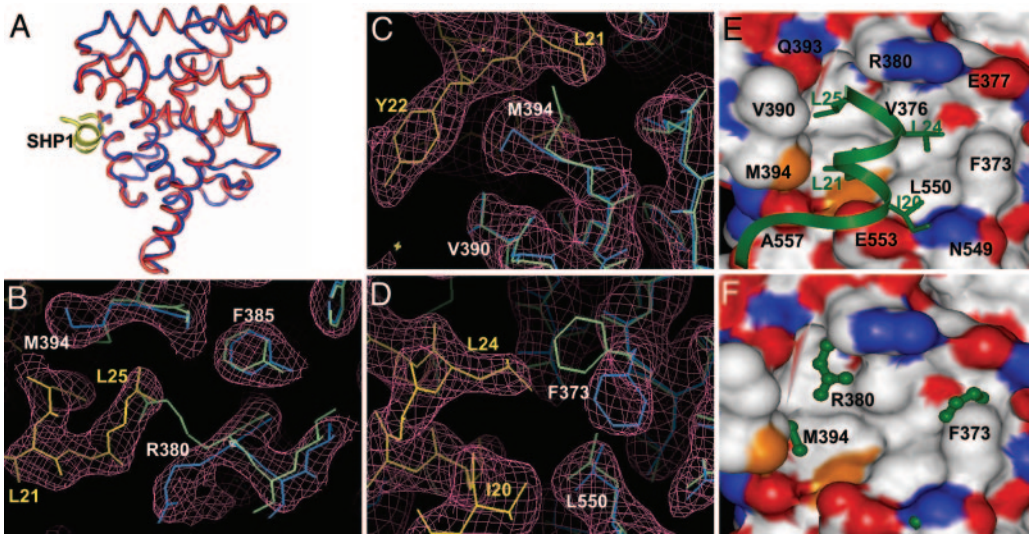

Fig. 3. Conformational changes of LRH-1 induced by SHP binding. (*A*) Superposition of the apo-LRH-1 (blue) with the LRH-1/SHP complex, where LRH-1 is colored in red and SHP in yellow. (*B–D*) Conformational changes of the side chain in the LRH-1 residues involved in binding of the SHP ID1 motif. The apo-LRH-1 is shown in green, the SHP-bound LRH-1 is in blue, and the SHP is in yellow. The electron density is shown in purple at 1σ contoured level. (*E*) Docking mode of the SHP ID1 motif on to the surface of the LRH-1 coactivator-binding site. (*F*) Surface topology of the cofactor-binding site of the LRH-1/SHP complex as distorted by the side chains of the apo-LRH-1 (green).

chain conformation of R380 (Fig. 3*B*). In the apo structure, the extended R380 side chain traces along the coactivator-binding site into the space that is normally occupied by L + 5 (L25) of the LXXLL motif. In response to SHP binding, the side chain of R380 is moved 5–8.0 Å to open up the pocket for the L + 5 of the LXXLL motif. Side chains of residues F373, M394, and N549 are also moved 4–5 Å away from their corresponding positions in the apo structure to accommodate the binding of L + 4, L + 1, and I − 1 of the SHP LXXLL motif (Fig. 3 *C* and *D*). In addition to these major changes in the side chain conformations, the LRH-1 AF-2 helix is also shifted 0.5 Å, which extends the length of the charge clamp pocket to accommodate the binding of the SHP helix. These conformational changes dramatically alter the surface topology of the LRH-1 coactivator-binding site (Fig. 3*F*) and thus allow the receptor to interact with SHP with high affinity.

Determinants of the SHP Binding to LRH-1. To determine the role of each residue of the SHP ID1 and ID2 peptides in binding to LRH-1, we performed peptide competition experiments with alanine scan mutants (Fig. 4*A*). Replacement of the two core interface residues (L + 1 and L + 5) resulted in >150-fold decrease in the binding affinity of both SHP motifs to LRH-1, in agreement with the central role of these two SHP residues in the binding to LRH-1. Mutations in I − 1 and L + 4, which comprise the peripheral interface, also moderately decrease SHP binding. Interestingly, mutations in the +3 and +7 residues increase SHP binding to LRH-1 by 5- to 10-fold. These residues do not contact LRH-1 directly, but the alanine mutations can increase the helical propensity of the SHP sequence (30), and thus stabilize the docking of the SHP helix.

To assess the importance of these two SHP motifs in the repression of LRH-1, we mutated either motif in the context of the full-length SHP and performed cell-based assays by using an LRH-1/SF-1 reporter. Fig. 4*B* shows that wild-type SHP can repress LRH-1 activity to baseline levels, and mutations in the SHP ID1 motif have little effect on SHP repression function. In contrast, mutations in the SHP ID2 motif abolish the ability of SHP to repress LRH-1, which demonstrates that the functional interaction between SHP and LRH-1 is mediated through the SHP ID2 motif despite the finding that both SHP motifs bind to LRH-1 with approximately the same affinity.

The transcriptional activity of SF-1, a receptor closely related to LRH-1, is not inhibited by SHP but is repressed by Dax-1, a tissue-specific repressor of SF-1 (Fig. 4*C*). The SHP ID1 and ID2 peptides interacted with purified SF-1 LBD with IC_{50} values of 11 μM and 33 μM, respectively (Fig. 4*D*). This binding affinity is roughly 20- to 80-fold weaker than the binding of the SHP motifs to LRH-1 or the binding of the second and third motifs of Dax-1 to SF-1 (Fig. 4*D*). In fact, the biotinylated SHP ID2 peptide showed no interaction with SF-1 in conditions in which both TIF2 and SHP ID1 interacted with SF-1 (Fig. 4*E*). Importantly, a mutated mouse SHP in which the SHP ID2 motif is replaced with the third Dax-1 motif (SF-1 + SWAP in Fig. 4*C*) represses SF-1 activation as efficiently as Dax-1. These data suggest that the insensitivity of SF-1 to SHP repression can be attributed in part to its poor binding to the SHP ID2 motif. The transcriptional activity of LRH-1 is also severely inhibited by Dax-1 as well as by the SHP swap mutant (Fig. 4*C*), consistent with the finding that all three Dax-1 motifs interact well with LRH-1 (Fig. 5*E*). The higher affinity of the three Dax-1 motifs for LRH-1 compared with SF-1 is surprising but consistent with a previous report (31) showing that all three Dax-1 motifs interact strongly with LRH-1 and that Dax-1 mediates stronger repression on LRH-1 than on SF-1. The coexpression of LRH-1 with SF-1 and Dax-1 in steroidogenic tissues (32, 33) and the strong interactions between LRH-1 and Dax-1 suggest that LRH-1 is also a physiological target for Dax-1.

Basis of the SHP Selectivity Between LRH-1 and SF-1. To understand the basis for the selective interaction between SHP and LRH-1, we

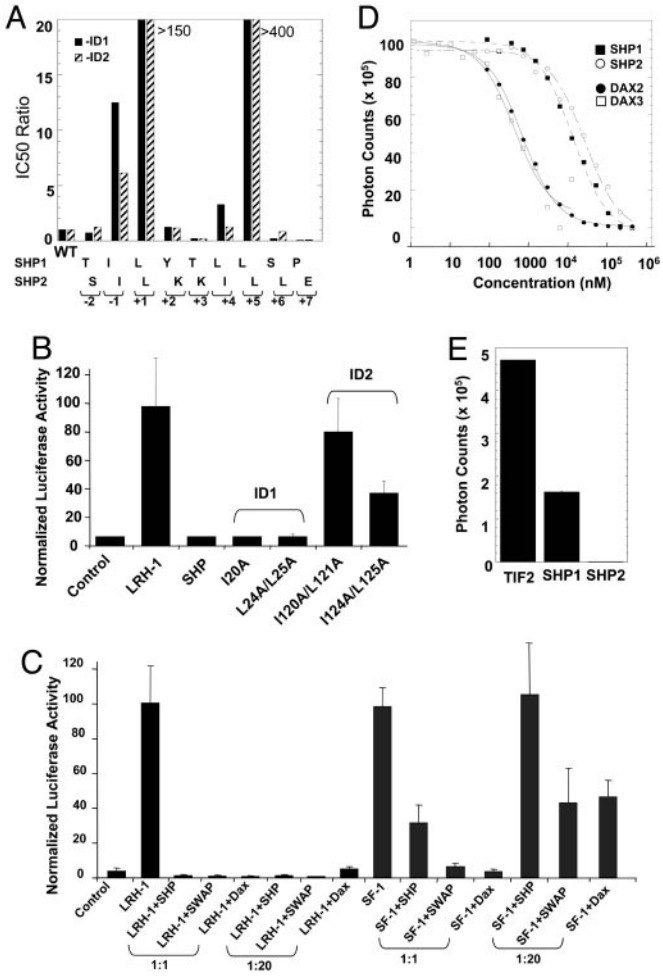

Fig. 4. Determinants and functional correlation of the LRH-1/SHP interactions. (*A*) Effects of alanine scanning mutations of the SHP ID1 and ID2 motifs on their binding to LRH-1 as determined by AlphaScreen. IC_{50} ratios are determined between the values of mutated peptides and the IC_{50} values for the wild-type SHP ID1 and ID2 motifs. (*B*) Effects of the mutations of the SHP ID1 and ID2 motifs on repression of LRH-1 in cell-based reporter assays. The amount of the expressing plasmids of SHP and LRH-1 is 2 ng and 40 ng, respectively (1:20 ratio). The luciferase activity for the transfections performed with LRH-1 alone was normalized to 100%. (*C*) Direct comparison of repression of LRH-1 and SF-1 by SHP and Dax-1 in cell-based reporter assays. The amount of the mouse SHP, mouse Dax-1, and the SHP SWAP expression vector is either 40 ng (1:1 ratio to LRH-1 or SF-1) or 2 ng in the repression assays (1:20 ratio to LRH-1 or SF-1). SWAP represents the SHP mutant containing K122Y/K123S/I124L/E126T/E127S/P128S that replace the SHP ID2 motif with the Dax-1 third motif. The luciferase activities for the transfections performed with LRH-1 and SF-1 alone were normalized to 100%. (*D*) Binding affinity of the SHP motifs and the Dax-1 motifs to SF-1 as determined by peptide competition experiments by using AlphaScreen. The IC_{50} of the second and the third motifs of Dax-1 is ≈500 nM vs. 10–40 μM for the two SHP motifs. (*E*) No binding of the biotinylated SHP ID2 motifs to SF-1 as compared with the binding of the TIF2 and SHP ID1 motif to SF-1.

performed structural comparison of the LRH-1/SHP complex with our recent structure of the SF-1/SHP/phospholipid complex (PDB code 1YP0) (34, 39). Although the Cα atoms comprising the coactivator-binding site overlap exceedingly well between LRH-1 and SF-1 (rmsd < 0.5 Å), there are three major differences in their coactivator binding sites (Fig. 5*A*). The first and most pronounced difference is the change in LRH-1 residues L372 and F373, which form part of the pockets for I − 1, L + 1, and L + 4 of the LXXLL motif, to F274 and I275 in SF-1. The second difference is the

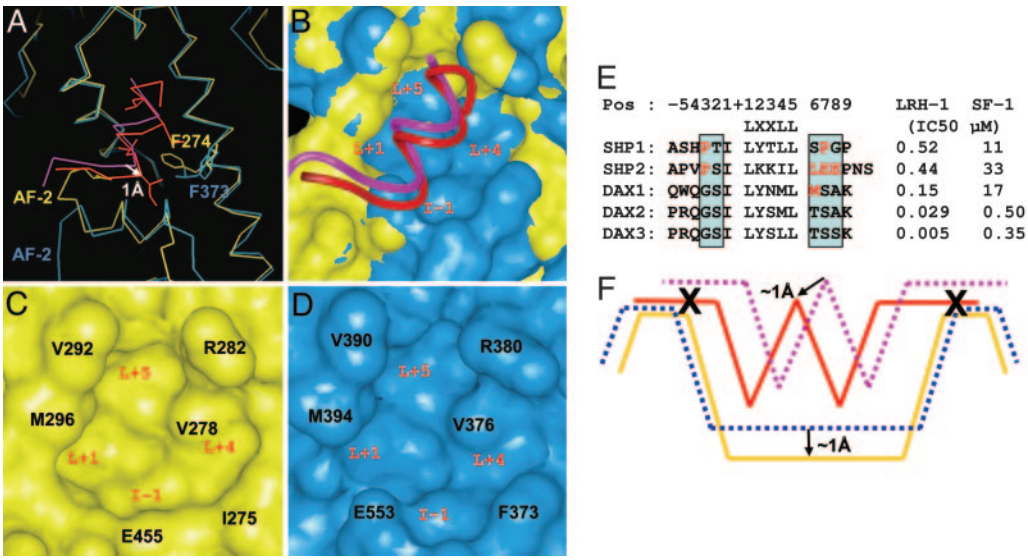

Fig. 5. Basis for the SHP selectivity between LRH-1 and SF-1. (*A*) An overlap of the LRH-1 (blue) with the SF-1 (yellow) showing the difference of their coactivator-binding site and the docking mode of the SHP helix. The SHP ID1 motif in the LRH-1 and SF-1 is shown in pink and red, respectively. Key differences in their residues, the AF-2 helix and the shift of the SHP helix are noted. (*B–D*) Surface topology of the LRH-1 (blue) and SF-1 (yellow) coactivator-binding site showing a narrow but deep site in SF-1 (*C*), and a wide but shallow site in LRH-1 (*D*). The pocket for adopting the SHP LXXLL residues are noted in red, and key SF-1 and LRH-1 residues are noted in black. The differences between the coactivator-binding site of LRH-1 and SF-1 are further illustrated by an overlay of their surfaces in *B*, which shows that the center of the coactivator-binding site is mostly covered by LRH-1 (blue), whereas the flanking ridge is mostly covered by SF-1 (yellow). (*E*) The binding affinity (IC_{50}) of various SHP and Dax LXXLL motifs to LRH-1 and SF-1 as determined by peptide competitions. The residues that affect the binding affinity to SF-1 are in red. (*F*) A model for the SHP selectivity between LRH-1 and SF-1. The SF-1/SHP model is shown in yellow/red solid lines and the LRH-1/SHP is shown in blue/pink dashed lines. The 1.0-Å shift of the SHP helix into the SF-1 pocket (yellow) is also indicated.

orientation of the protein tail after the AF-2 helix. In LRH-1, the AF-2 tail is pointed away from the coactivator-binding site, whereas the SF-1 AF-2 tail is oriented toward it. The third difference is the shift of the SF-1 AF-2 helix and its preceding loop toward the right side of the LBD (Fig. 5*A*).

Together, these differences significantly alter the surface topology of the SF-1 coactivator-binding site (Fig. 5 *B–D*) and consequently the docking mode of the SHP LXXLL motif. Compared with LRH-1, the SF-1 coactivator-binding site is narrower and deeper (Fig. 5 *C* and *D*), thus allowing the SHP helix to dock ≈1 Å deeper into the pocket (Fig. 5 *A* and *B*). Because the ridge of the coactivator-binding site is about the same height in SF-1 and LRH-1, the deeper docking mode of the SHP helix into the SF-1 surface results in a collision between the residues flanking the SHP LXXLL motif and the ridge of the SF-1 coactivator-binding site (Fig. 5 *B* and *F*). The second and third LXXLL motifs of Dax-1 bind to SF-1 with 20- to 100-fold higher affinity than the SHP motifs (Fig. 5*E*), and inspection of their sequence reveals that the two Dax-1 motifs contain small residues flanking their LXXLL core (GS at −3 and −2; and TSA/S at +6, +7, and +8). In contrast, the SHP LXXLL motifs are surrounded by large side chain residues. The preference of SF-1 for smaller flanking residues is made evident by comparing the first and the second motifs of Dax-1 (DAX1 and DAX2 in Fig. 5*E*). These two Dax-1 motifs contain identical amino acids from positions −4 to +9 except for the residue at position +6, where DAX1 has a large side chain residue methionine and DAX2 has a smaller threonine. The binding affinity of DAX2 to SF-1 is >30-fold stronger than DAX1, supporting the important role of the flanking sequence of the LXXLL motif in binding to SF-1.

Discussion

Repression of LRH-1 transcriptional activity by the atypical corepressor SHP regulates key aspects of cholesterol homeostasis (2, 3). Mice lacking SHP show imbalances in bile acid metabolism and abnormal responses when challenged with diets enriched in cholesterol and/or cholic acid (35, 36). In this report, we provide a structural and biochemical characterization of the binding of the two SHP LXXLL-related motifs to LRH-1. The crystal structure of the LRH-1/SHP complex reveals that LRH-1 adopts a canonical active conformation and that SHP binding results in conformational changes in LRH-1. Our mutagenesis and binding studies show that only the second SHP motif is required for repressing LRH-1, and this motif displays a marked preference for LRH-1 over SF-1 due to collisions between the SHP residues flanking the core LXXLL motif and the SF-1 coactivator-binding site. These results provide a structural model for understanding the high affinity and selective interaction between SHP and LRH-1.

Consistent with its constitutive activation properties, LRH-1 is able to interact with a number of coactivator LXXLL motifs in the absence of any exogenous ligand (Fig. 1*B*). The structure of the LRH-1/SHP complex reveals that LRH-1 is folded into the active conformation despite the empty ligand-binding pocket, like the apo LRH-1 structure (10). Based on the apo LRH-1 structure, it was proposed that the coactivator-binding site of LRH-1 is not optimized for binding to LXXLL coregulator motifs (10, 18). Contrary to this notion, our quantitative competition experiments reveal that LRH-1 is capable of interacting with a number of coactivator motifs with moderate to high affinity. In addition, the two SHP motifs show preferential binding to LRH-1 over a number of other receptors, including HNF4α, PPARs, ERs, and oxosteroid hormone receptors (Fig. 1*D*). The higher affinity of SHP for LRH-1 compared with these other receptors suggests a reason why LRH-1 target genes such as CYP7A1 and CYP8B1 are especially sensitive to the repressive actions of SHP (35, 36).

In response to SHP binding, several side chains that comprise the LRH-1 coactivator-binding site undergo significant conformational changes, which dramatically alters the topology of the binding site to accommodate the SHP helix. The docking mode of the SHP helix is analogous to the docking of coactivator LXXLL motifs in other nuclear receptors, with the hydrophobic leucines in the +1 and +5 positions oriented toward the central interface with LRH-1. Alanine mutations in these residues

demonstrate their critical role in binding to the receptor (Fig. 4*A*). The charge clamp that caps both ends of the SHP helix is comprised in part by R380 from helix H3 instead of the lysine typically found in other nuclear receptors. The larger side chain of R380 seems to form a better shielded pocket for docking of L + 5 of the SHP motifs, thus increasing the affinity of SHP binding to LRH-1.

Despite the similar affinity of the two SHP motifs for LRH-1, only mutations in the SHP ID2 motif abolish SHP repression of LRH-1 (Fig. 4*B*). This result is consistent with previous findings showing that mutations in the SHP ID2 motif but not in the ID1 motif are sufficient to abolish SHP inhibition of GR and AR (25, 37). Thus, the same motif is required for interactions with both monomeric and dimeric receptors. Modeling studies indicate that the SHP ID2 motif is located within the two β-strands between helices H5 and H6, where the ILKKIL sequence is exposed to solvent and well positioned to interact with the coactivator-binding site of LBDs. Interestingly, SF-1, an LRH-1 paralog, is not repressed by SHP but is repressed by Dax-1. Consistent with this result, our peptide-binding assays reveal that the two Dax-1 LXXLL motifs bind well to SF-1 but that the SHP ID2 motif interacts poorly with SF-1 (Fig. 4*E* and 5*E*). Furthermore, swapping the SHP ID2 motif with the Dax-1 third motif allows SHP to repress SF-1 to the same degree as Dax-1. Thus, the differential effects of SHP on LRH-1 and SF-1 can be attributed in part to the selective binding of the SHP ID2 motif to LRH-1.

A basis for the differential binding of the SHP motif to LRH-1 and SF-1 becomes evident by comparing the surface topology of their coactivator-binding sites (Fig. 5). The coactivator-binding site in LRH-1 is wide and well formed, which is consistent with the ability of LRH-1 to interact with various LXXLL motifs with high affinity (Fig. 1*B* and 5*E*). In contrast, the coactivator-binding site in SF-1 is narrower and deeper, which may explain why SF-1 interacts with fewer LXXLL motifs. The deeper SF-1 coactivator-binding site forces the SHP LXXLL helix to dock $\approx$1 Å closer to the pocket than the SHP helix in LRH-1. This docking mode selects for LXXLL motifs with smaller adjacent residues, which otherwise would collide with the ridge of the SF-1 coactivator-binding site. Thus, selectivity for the SF-1 coactivator cleft is encoded by the residues neighboring the core LXXLL motif (Fig. 5 *E* and *F*). This model is supported by the presence of small residues flanking the second and third LXXLL motifs in Dax-1, which binds to SF-1 with high affinity. Consistent with this model, point mutations that change S − 2 or T + 6 to large residues in the Dax-1 third motif severely reduce its binding to SF-1 (31). A mechanistic understanding of how cofactors are selectively recruited by nuclear receptors has been a challenge, given the numerous LXXLL motifs, which adopt essentially the same two-turn α-helix in all LBD structures solved to date (reviewed in ref. 38). Our previous studies revealed that a subset of nuclear receptors including GR and CAR use a second charge clamp to achieve selective binding to TIF2 (24, 29). In contrast, we now provide evidence that the different surface topologies of the LRH-1 and SF-1 coactivator-binding sites define their selectivity for the sequence flanking the core LXXLL motifs. These results illustrate that nuclear receptors can employ diverse structural mechanisms to achieve specific recognition of their physiological coregulators.

We thank K. L. Parker (University of Texas Southwestern Medical School), B. O'Malley (Baylor College of Medicine, Houston), D. McDonnell (Duke University, Durham, NC), T. Willson (GlaxoSmith-Kline, Research Triangle Park, NC), and E. Willson (University of North Carolina, Chapel Hill) for cDNAs of various receptors and compounds, W. D. Tolbert and J. S. Brunzelle for assistance in data collection at sector 32 of the Advance Photo Source, D. Petillo for DNA sequencing, and W. Minor (University of Virginia, Charlottesville) for the HKL2000 package. Use of the Advanced Photon Source was supported by the Office of Science of the U.S. Department of Energy. H.E.X. acknowledges the generosity of the Jay and Betty Van Andel Foundation, the National Institutes of Health (NIH) Nuclear Receptor Signaling Atlas (NURSA) orphan receptor program (Grant U19DK62434-01), and the Michigan Economic Development Corporation and the Michigan Technology Tri-Corridor (Grant 085P1000817). M.C. and S.A.K. were supported by Robert A. Welch Foundation Grant I-1558.

1. Fayard, E., Auwerx, J. & Schoonjans, K. (2004) *Trends Cell Biol*. **14,** 250–260.
2. Goodwin, B., Jones, S. A., Price, R. R., Watson, M. A., McKee, D. D., Moore, L. B., Galardi, C., Wilson, J. G., Lewis, M. C., Roth, M. E., *et al*. (2000) *Mol. Cell* **6,** 517–526.
3. Lu, T. T., Makishima, M., Repa, J. J., Schoonjans, K., Kerr, T. A., Auwerx, J. & Mangelsdorf, D. J. (2000) *Mol. Cell* **6,** 507–515.
4. Delerive, P., Galardi, C. M., Bisi, J. E., Nicodeme, E. & Goodwin, B. (2004) *Mol. Endocrinol*. **18,** 2378–2387.
5. Chen, F., Ma, L., Dawson, P. A., Sinal, C. J., Sehayek, E., Gonzalez, F. J., Breslow, J., Ananthanarayanan, M. & Shneider, B. L. (2003) *J. Biol. Chem*. **278,** 19909–19916.
6. Schoonjans, K., Annicotte, J. S., Huby, T., Botrugno, O. A., Fayard, E., Ueda, Y., Chapman, J. & Auwerx, J. (2002) *EMBO Rep*. **3,** 1181–1187.
7. Parker, K. L., Rice, D. A., Lala, D. S., Ikeda, Y., Luo, X., Wong, M., Bakke, M., Zhao, L., Frigeri, C., Hanley, N. A., *et al*. (2002) *Recent Prog. Horm. Res*. **57,** 19–36.
8. Sadovsky, Y. & Dorn, C. (2000) *Rev. Reprod*. **5,** 136–142.
9. Wilson, T. E., Fahrner, T. J. & Milbrandt, J. (1993) *Mol. Cell. Biol*. **13,** 5794–5804.
10. Sablin, E. P., Krylova, I. N., Fletterick, R. J. & Ingraham, H. A. (2003) *Mol. Cell* **11,** 1575–1585.
11. Lee, Y. K. & Moore, D. D. (2002) *J. Biol. Chem*. **277,** 2463–2467.
12. Seol, W., Choi, H. S. & Moore, D. D. (1996) *Science* **272,** 1336–1339.
13. Nishizawa, H., Yamagata, K., Shimomura, I., Takahashi, M., Kuriyama, H., Kishida, K., Hotta, K., Nagaretani, H., Maeda, N., Matsuda, M., *et al*. (2002) *J. Biol. Chem*. **277,** 1586–1592.
14. Lee, Y. K., Dell, H., Dowhan, D. H., Hadzopoulou-Cladaras, M. & Moore, D. D. (2000) *Mol. Cell. Biol*. **20,** 187–195.
15. Seol, W., Hanstein, B., Brown, M. & Moore, D. D. (1998) *Mol. Endocrinol*. **12,** 1551–1557.
16. Lee, Y. K., Parker, K. L., Choi, H. S. & Moore, D. D. (1999) *J. Biol. Chem*. **274,** 20869–20873.
17. Johansson, L., Bavner, A., Thomsen, J. S., Farnegardh, M., Gustafsson, J. A. & Treuter, E. (2000) *Mol. Cell. Biol*. **20,** 1124–1133.
18. Xu, P. L., Liu, Y. Q., Shan, S. F., Kong, Y. Y., Zhou, Q., Li, M., Ding, J. P., Xie, Y. H. & Wang, Y. (2004) *Mol. Endocrinol*. **18,** 1887–1905.
19. Otwinowski, Z. & Minor, W. (1997) *Methods Enzymol*. **276,** 307–326.
20. Gampe, R. T., Jr., Montana, V. G., Lambert, M. H., Miller, A. B., Bledsoe, R. K., Milburn, M. V., Kliewer, S. A., Willson, T. M. & Xu, H. E. (2000) *Mol. Cell* **5,** 545–555.
21. Navaza, J., Gover, S. & Wolf, W. (1992) in *Molecular Replacement: Proceedings of the CCP4 Study Weekend*, ed. Dodson, E. J. (SERC, Daresbury, U.K.), pp. 87–90.
22. Brunger, A. T., Adams, P. D., Clore, G. M., DeLano, W. L., Gros, P., Grosse-Kunstleve, R. W., Jiang, J. S., Kuszewski, J., Nilges, M., Pannu, N. S., *et al*. (1998) *Acta Crystallogr. D Biol. Crystallogr*. **54,** 905–921.
23. Xu, H. E., Stanley, T. B., Montana, V. G., Lambert, M. H., Shearer, B. G., Cobb, J. E., McKee, D. D., Galardi, C. M., Plunket, K. D., Nolte, R. T., *et al*. (2002) *Nature* **415,** 813–817.
24. Suino, K., Peng, L., Reynolds, R., Li, Y., Cha, J. Y., Repa, J. J., Kliewer, S. A. & Xu, H. E. (2004) *Mol. Cell* **16,** 893–905.
25. Borgius, L. J., Steffensen, K. R., Gustafsson, J. A. & Treuter, E. (2002) *J. Biol. Chem*. **277,** 49761–49766.
26. Ourlin, J. C., Lasserre, F., Pineau, T., Fabre, J. M., Sa-Cunha, A., Maurel, P., Vilarem, M. J. & Pascussi, J. M. (2003) *Mol. Endocrinol*. **17,** 1693–1703.
27. Bae, Y., Kemper, J. K. & Kemper, B. (2004) *DNA Cell Biol*. **23,** 81–91.
28. Nolte, R. T., Wisely, G. B., Westin, S., Cobb, J. E., Lambert, M. H., Kurokawa, R., Rosenfeld, M. G., Willson, T. M., Glass, C. K. & Milburn, M. V. (1998) *Nature* **395,** 137–143.
29. Bledsoe, R. K., Montana, V. G., Stanley, T. B., Delves, C. J., Apolito, C. J., McKee, D. D., Consler, T. G., Parks, D. J., Stewart, E. L., Willson, T. M., *et al*. (2002) *Cell* **110,** 93–105.
30. Padmanabhan, S., Marqusee, S., Ridgeway, T., Laue, T. M. & Baldwin, R. L. (1990) *Nature* **344,** 268–270.
31. Suzuki, T., Kasahara, M., Yoshioka, H., Morohashi, K. & Umesono, K. (2003) *Mol. Cell. Biol*. **23,** 238–249.
32. Boerboom, D., Pilon, N., Behdjani, R., Silversides, D. W. & Sirois, J. (2000) *Endocrinology* **141,** 4647–4656.
33. Wang, Z. N., Bassett, M. & Rainey, W. E. (2001) *J. Mol. Endocrinol*. **27,** 255–258.
34. Li, Y., Choi, M., Cavey, G., Daugherty, J., Suino, K., Kovach, A., Bingham, N. C., Kliewer, S. A. & Xu, H. E. (2005) *Mol. Cell* **17,** 491–502.
35. Wang, L., Lee, Y. K., Bundman, D., Han, Y., Thevananther, S., Kim, C. S., Chua, S. S., Wei, P., Heyman, R. A., Karin, M. & Moore, D. D. (2002) *Dev. Cell* **2,** 721–731.
36. Kerr, T. A., Saeki, S., Schneider, M., Schaefer, K., Berdy, S., Redder, T., Shan, B., Russell, D. W. & Schwarz, M. (2002) *Dev. Cell* **2,** 713–720.
37. Gobinet, J., Auzou, G., Nicolas, J. C., Sultan, C. & Jalaguier, S. (2001) *Biochemistry* **40,** 15369–15377.
38. Li, Y., Lambert, M. H. & Xu, H. E. (2003) *Structure (Camb.)* **11,** 741–746.
39. Krylova, I. N., Sablin, E. P., Moore, J., Xu, R. X., Waitt, G. M., MacKay, J. A., Juzumiene, D., Bynum, J. M., Madauss, K., Montana, V., *et al.* (2005) *Cell* **120,** 343–355.